Direct measurement of the total reaction rate of OH in the atmosphere

B. Calpini, F. Jeanneret, M. Bourqui, A. Clappier, R. Vajtai* and H. van den Bergh

Swiss Federal Institute of Technology (EPFL), LIDAR Group, Ecublens, 1015 Lausanne, Switzerland

A new method to investigate atmospheric chemical kinetics is presented. It is based on the pump and probe principle. Preliminary measurements are described on the decay rate of OH in the planetary boundary layer after its concentration has been raised by laser flash photolysis of background ozone and subsequent reaction of the O(1D) with atmospheric water vapor. The measured OH disappearance kinetics are compared with model calculations yielding information on the fast reaction of OH. The presented point measurements can be extended to a range resolved differential absorption LIDAR technique.

In tropospheric chemistry, OH plays a key role. For instance it is essential in converting many trace species from water-insoluble to water-soluble forms, thus assisting in their deposition rate. Due to OH high reactivity, its concentration in the planetary boundary layer (PBL) is very low, at most of the order of 10^6 radicals cm^{-3}. Thus routine measurement of its steady state concentration for comparison with model calculations is non trivial [1,2]. Furthermore, even in the more complete models there still remains some uncertainty as to some of the sources and sinks of OH. Among others it is still somewhat unclear where all the HONO comes from that acts as an early daytime source of OH. Furthermore it is not likely that as yet all the multitude of hydrocarbons that act as non-negligible sinks have been identified.

In the present paper we propose a method for investigating the fast kinetics of OH *in situ* in the atmosphere using a perturbation technique in which high concentration of OH are created by the laser flash photolysis of atmospheric O_3 followed by the reaction of $O(^1D)$ with H_2O. Typically we have locally enhanced the hydroxyl radical concentration by 5 orders of magnitude. Thus the OH is easier to detect and its fast disappearance can be followed over a sufficient time period to try to quantify the reaction kinetics. As we shall discuss below, this fast OH kinetics can be reduced to contributions from a small number of reactions, essentially with CO, O_3, various volatile organic compounds (VOC), NO_x and the reaction with OH itself. Consequently if we simultaneously measure the concentrations of CO, O_3 and NO_x with the overall OH kinetics, we shall be able to deduce a total hydrocarbon reactivity $\Sigma k_i[OH]\,[VOC_i]$ from the difference between the measured overall OH decay rate and the sum of the reaction rates with CO, O_3, NO_x and OH itself. In a controlled atmosphere with known $\Sigma k_i[OH]\,[VOC_i]$, one can check for possible unknown fast OH reactions. Hence we shall be able to deduce if the fast kinetics of OH in the atmosphere is complete and well understood under condition that the measurements are sufficiently accurate. A final reason for undertaking these measurements of the fast kinetics of OH was that it seemed like a reasonable first choice to test the pump and probe technique for obtaining new information on atmospheric chemistry. Below we describe the experimental method in some detail, and we compare the measured kinetics with those obtained in a model calculation. Experimental data are presented both from controlled atmospheres with known concentrations of chemical constituents, and from the natural PBL. We also mention the possibility of extending these perturbation kinetics measurements from the *in situ* case to the range resolved remote sensing case, using a DIfferential Absorption Lidar (DIAL) technique. Finally it will be briefly discussed that measurement of $\Sigma k_i[OH]\,[VOC_i]$ could possibly lead to information on local NO_x *versus* VOC limiting of the production of tropospheric ozone.

Experimental setup

A diagram of the instrument is shown in figure 1. The major parts are: a) the pump laser for the flash photolysis beam used to create the high concentration of OH, b) the probe beam for detecting the OH by laser induced fluorescence (LIF), c) the OH fluorescence cell, d) the timing unit and e) the detector and data acquisition system.

(a) Pump laser: The pump laser is a 10 Hz frequency quadrupled Nd:YAG laser (Continuum SureLight-III-10). Its energy is 55 mJ/pulse with a pulse duration of 4 ns FWHM. The beam is directed into the gas flow in the reaction cell via three dichroic mirrors, a Pellin-Broca prism, and a right angle prism. The pump beam energy remaining at the reaction site is 18 mJ, and the beam has a circular shape with

*Actual address: JATE University, Department of Experimental Physics, Szeged, H-6720 Szeged, Hungary.

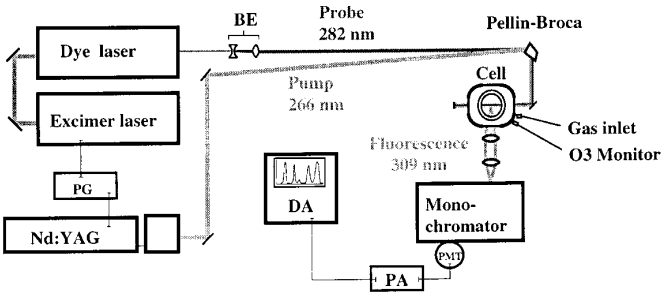

Figure 1. Schematic diagram of the experimental setup. BE - beam expander; PMT - photomultiplier tube; PA - (fast, low-noise) preamplifier; DA - data acquisition; PG - pulse generator.

10 mm diameter. With a quantum yield for $O(^1D)$ in the ozone photolysis of 0.88 [3], and an ozone absorption cross section at 266 nm $\sigma_{O3}(266\ nm) = 948.5 \times 10^{-20}\ cm^2$ [4], about 23% of the ozone is transformed to $O(^1D)$. Thus OH is formed by the reactions:

$$O_3 \xrightarrow{h\nu(266\ nm)} O(^1D) + O_2\ (^1\Delta g) \quad (1)$$

$$O(^1D) + H_2O \rightarrow 2OH \quad (2)$$

In equation (2) $O(^1D)$ reacts with water vapor to form OH, but it is also deactivated to $O(^3P)$ in collision with H_2O itself and other gases among which mainly nitrogen and oxygen. With a gas mixture of 90% N_2, 8% O_2 and 2% H_2O, and quenching rate constants of respectively 2.6×10^{-11}, 4.0×10^{-11} and $19.5 \times 10^{-11}\ cm^3\ mol^{-1}\ s^{-1}$ [5, 6], only 12% of the $O(^1D)$ reacts with water vapor. If we add 50 ppb O_3 to this mixture, the simulated [OH] reaches 6% of the initial $[O_3]$, i.e. 7.2×10^{10} molecules cm^{-3} at standard atmospheric conditions. This value is about 5 orders of magnitude higher than the maximum [OH] found in the PBL, thus making the [OH] detection simple in the pump and probe experiment as compared to the *in situ* "steady state" measurements [7–12, 2]. It should be noted that part of the pump beam laser energy at 266 nm can in principle be directly absorbed by atmospheric compounds other than ozone, and in particular by some of the important aromatic volatile organic compounds. In order to address this problem in more detail, the pump laser source at fixed wavelength will in the future be soon replaced by a tuning excimer dye laser source, in order to try to find pump beam wavelengths at which this unwanted photochemistry can be minimized. This will be done in controlled atmosphere experiments with known concentrations of various absorbing hydrocarbon additives.

(b) Probe laser: A grating tuned, pulsed dye laser (Lambda Physik LPD 3002) is pumped by a XeCl excimer laser (Lambda Physik LPX210i at 308 nm, with 400 mJ/pulse). The dye is Coumarin 153 (Radiant dye, 4.2 g/L for the oscillator and 1.4 g/L for the amplifier) in methanol. The Coumarin is mixed 1:1 with DABCO (1,4-Diazabicyclo[2.2.2]-octan, 98%) which almost double the life time of the dye. The dye has a maximum wavelength conversion efficiency of 16% near 540 nm. With a BBO-I type frequency doubler crystal followed by 4 Pellin-Broca prisms for the UV/fundamental separation, one obtains a UV tunable light source between 281 and 284 nm, with a resolution better than 0.2 cm^{-1} (laser bandwidth of 0.014 Å) and a 0.01 Å wavelength tuning step. Its energy is set at 0.58 mJ $pulse^{-1}$ in the fluorescence cell. A beam expander ($2x$) is used to make the beam more parallel with a diameter of 4 mm at the reaction site.

Under these experimental conditions, the possibility of saturation of the OH signal was checked by using a set of different neutral density filters. Thus we showed experimentally that no saturation occurred. Furthermore calculation of the probe beam efficiency gives an estimate of 86% thus indicating that the saturation is avoided.

The pump and the probe beams are both horizontally polarized and combined by feeding them at the appropriate angles into the Pellin-Broca prism. Careful alignment superposes the two beams both in the near and far field at the exit of the prism. This arrangement is preferred to the classic crossed beam experiment, as the same optical layout has been used in the coaxial range resolved DIAL scheme.

(c) Fluorescence cell: A black anodized aluminum cell with a square cross section (dimensions: $300 \times 100 \times 100\ mm^3$) is fitted with different plug-in gas inlets for dry air, O_3, N_2, O_2, H_2O, CH_4, NO_x, and other gases on its entrance side. This cell is evacuated from the opposite side. At the center of the cell, two flanges perpendicular to the vertical axis support UV anti-reflection coated quartz windows which transmit both the pump and probe laser beams. The OH fluorescence passes through a 3rd quartz window in the vertical plane. A 4th flange holds the temperature probe together with other gas feedthroughs, one of which is used to pump a small fraction of the air stream from the reaction site to an ozone UV absorption monitor (HORIBA APOA-350E). Ozone is produced by an ozone generator at a flow rate of 2.5 L/min of air and its concentrations range from 100 to 700 ppb at the generator exit, gives 70 to 400 ppb at the reaction site as measured by the ozone detector. Dry N_2 is added to the gas flow as a buffer gas, and the synthetic air contains a mixture N_2:O_2:H_2O = 90:8:2. The total gas pressure is one atmosphere. In the cell, a temperature controlled water container keeps the water vapor to 2%. At this point of the study, no detailed analysis of trace gas contaminations is performed on this synthetic air mixture. It should be noted that any residue of for instance reactive hydrocarbons in the cell can strongly decrease the OH life time and hence increase the apparent rate coefficient for a given constituent. Such effect is shown to remain negligible when the experiment is performed with a specific pollutant at high concentration in the stream.

(d) Timing unit: The Nd:YAG laser is run in its internal trigger mode at 10 Hz, and a photodiode collecting a reflection of this light triggers a pulse generator (Stanford Research DG535). The latter triggers the excimer laser with

a time delay between the pump and the probe laser pulses selected between 1 and 100 ms, at a delay resolution of 1 ns.

(e) Detector and data acquisition system: The laser induced fluorescence signal is detected at 309 nm. Two lenses are used to collect and transport the light from the fluorescence cell to the entrance slit of a double grating monochromator (Jobin Yvon DH 10, with the two gratings blazed at 250 nm and with 2×10^{-9} stray light rejection). The lenses also match the F 3.5 numerical aperture. With the entrance, the middle and the exit slit width of 1, 2 and 1 mm respectively, a resolution of 4 nm is obtained. The LIF signal at 309 ± 2 nm is detected by a side-on photo-multiplier tube (1P28 Hamamatsu). The electronic output signal is preamplified by a fast/low-noise 25 X amplifier (Stanford Res. SR 445) before it is stored in an 8 bit/125 MHz oscilloscope (LeCroy 9400). The latter is triggered by a PIN photodiode which takes its signal from the probe laser.

Sensitivity

Laser induced fluorescence spectroscopy (LIF) is a direct detection method. Hence the relationship between the analog signal on the oscilloscope and the OH concentration in molecules cm^{-3} depends on the sensitivity of the experimental setup and on the spectroscopic properties of the OH radical. The energy level diagram of the OH LIF measurement is presented in figure 2. The analog signal S_{OH} is measured as Volts on the AD oscilloscope and can be expressed in the following way:

$$S_{OH} = V \cdot \frac{\Delta\Omega}{\Omega} \cdot T \cdot f \cdot \left\{ Y_f \cdot \frac{\Delta N}{N} \cdot \varepsilon_\lambda \right\} \cdot U \cdot [OH] \qquad (3)$$

where $$Y_f = \frac{k_{10}[M]}{k_{F_1} + k_{Q_1}[M] + k_{10}[M]} \cdot \frac{k_{F_0}}{k_{F_0} + k_{Q_0}[M]} \qquad (4)$$

$$\varepsilon_\lambda = 1 - \exp\left\{ \sigma_{eff} \cdot \frac{E \cdot \lambda}{h \cdot c \cdot S} \right\} \qquad (5)$$

V detection volume [cm^{-3}]
$\Delta\Omega / \Omega$ fraction of the solid angle contributing to the detection
T transmission of the optics
f spectral fraction of the OH fluorescence collected (detection at 309 nm ± 2 nm)
Y_f fraction of excited OH $A^2\Sigma$, ν' = 1 that fluoresces from ν'= 0
$\Delta N / N$ fraction of OH molecules in the probe rotational state ($^2\Pi_{3/2}$, ν'' = 0, N'' = 1)
ε_λ efficiency of the OH excitation in the $Q_1(1)$ transition at 281.914 nm
U PMT efficiency (photocathode, gain, preamplification) [V]
[OH] OH concentration [molecules cm^{-3}]

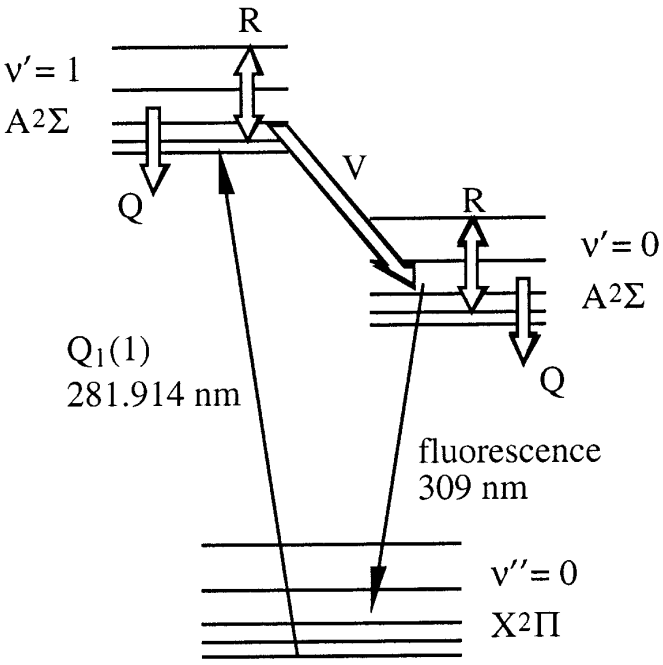

Figure 2. The laser-induced fluorescence (LIF) scheme used in the OH detection. The $A^2\Sigma^+$, ν' = 1, *N'* = 1 state is pumped with a laser pulse at 281.914 nm (Q_1(1) transition). This transition is followed by rotational energy redistribution in the ν' = 1 state and by collisional vibrational transfer *V* from ν' = 1 to ν' = 0. This is followed by rotational redistribution and finally by the fluorescence emitted from ν' = 0 down to ν'' = 0 which is collected at 309 nm. Quenching processes *Q* as well as the rotational transfer *R* decrease the fluorescence quantum yield at this wavelength.

k_{10} vibration energy transfer rate (1 ← 0) [cm^3 $molecule^{-1}$ s^{-1}]
k_Q electronic quenching rate constant [cm^3 $molecule^{-1}$ s^{-1}]
k_F fluorescence life time [s^{-1}]
$[M]$ number density of air mixture in the cell [molecules cm^{-3}]
σ_{eff} OH effective cross section [cm^2] at 281.914 nm
E LIF laser pulse energy [J]
λ excitation wavelength [cm]
h Planck constant [J s]
c speed of light [cm s^{-1}]
S laser beam cross sectional area [cm^2].

The OH concentration obtained from equation (3) with the parameters defined in table I is only a rough estimate, and the geometrical factors such as volume sampled for both pump and probe beams and solid angle of detection, as well as the optical efficiency of the experiment are difficult to evaluate with high precision. Statistical uncertainties have been obtained by repeating each data sample 10 times, each [OH] value being obtained from an average over 500 successive laser shots. Systematic errors are mainly due to the

Table I. Estimation of the different parameters introduced in equations (3-5) for the OH concentration and referenced values for the different quenching, vibrational and fluorescence rate constants included in the fluorescence quantum yield Y_f in equation (4).

V	0.0314 cm^3	±1%	Calculated
$\Delta\Omega$ / Ω	0.0156	±1%	Calculated
T	0.056	±2%	From manufacturer data sheet
f	0.76	±2%	Measured
Y_f	0.001	±10%	Calculated (cf. Tab. II)
ΔN / N	0.099	±5%	Calculated
ε_λ	0.78	±5%	Calculated
U	0.02 V	±1%	From manufacturer data sheet
σ_{eff}	2.8 10^{-16} cm^2	±10%	Calculated (cf. text)
E	580 µJ	±5%	Measured
λ	281.914 nm		Dieke et al., 1962
S	0.13 cm^2	±5%	Measured

	Rate coefficient 10^{-11} cm^3 s^{-1}		
Gas	k_{Q0}	k_{Q1}	k_{10}
N_2	2.6[a]	2.3[b]	23.3[a]
O_2	9.3[a]	22.5[b]	2.1[a]
H_2O	57[c]	16[c]	7.3[a]

[a] Williams 1996, [b] Burris 1988, [c] Chan 1983.

lasers and the optical alignment stability, and are difficult to estimate directly. By repeating different set of experimental conditions we found this systematic error on [OH] to be less than 5%. Finally the effective OH cross section used must be evaluated in detail. This cross section is calculated from the convolution of two distributions: a Gaussian distribution which contains the Doppler broadening and the probe laser bandwidth which has a FWHM of 1.6 pm, and a Lorentzian distribution containing the gas effective pressure broadening with a FWHM of 2.2 pm [13]. The convolution gives a Voigt profile with 3.07 pm FWHM from which a value of $\sigma_{eff} = 2.8 \times 10^{-16}$ cm^2 is derived for the effective OH cross section [14,15]. This value will be compared with the experimental value directly measured from the $Q_1(1)$ transition. All these sources of error result in an overall uncertainty for [OH] of 30%. Hence we compare our experimental [OH] with the theoretical value obtained from equations (1) and (2): for 50 ppb O_3 in 2% of water vapor, the $[OH]_{theoretical}$ formed is $[OH]_{theoretical} = (7.2 \pm 1.5) \times 10^{10}$ molecules cm^{-3}. For these initial experimental conditions, the resulting analog signal due to OH is 1.743 V. With the parameters introduced in equation 3 this leads to an experimental OH concentration $[OH]_{exp} = (7.6 \pm 2.3) \times 10^{10}$ molecules cm^{-3}.

Another fact must be considered: the OH formation due to the probe beam. At the probe wavelength (281.914 nm), O_3 absorbs with a cross section σ_{O3}(282 nm) = 325 × 10^{-20} cm^2 [4] or about one third of its value at 266 nm. The probe beam energy is 580 µJ and with a quantum yield of 0.95 [16], the concentration of OH formed by the probe beam amounts to 4.4% of the total [OH]. This may be compared with the experimental concentration obtained by measuring OH fluorescence without the pump beam. In this case the measured value is OH_{exp} = 0.084 V or 4.8% of the total OH signal obtained using both pump and probe laser beams. This secondary production of OH by the probe beam does not change with the varying delay time. Thus it is shown below that it does not influence the OH relaxation times significantly at the applied conditions, i.e. at times shorter than about 20 ms.

First experiments

In the present configuration of the experiment, the LIF detection system is designed to detect OH concentrations above 10^8 molecules cm^{-3}, which is about one and a half orders of magnitude higher than its maximum ambient concentration. Thus to optimize the apparatus, it was necessary to align the two beams and the LIF detection system by using an intense source of OH from a methane/oxygen gas burner. With the OH fluorescence signal from this flame, the different optical elements of the dye laser and the fluorescence detection optics were aligned. In a second step, the Nd:YAG laser beam exiting the Pellin-Broca prism is rendered coaxial with the dye laser beam.

The spectra obtained both from the flame experiment with only the LIF probe beam as excitation source (inset) as well as from the full pump and probe experiment using the reaction cell rather than the flame are shown in figure 3. The OH radicals are excited in *Q*- and *R*- branch lines of the (1,0) band. The fluorescence analyzing monochromator is positioned at 309 nm ± 2 nm. The fluorescence excitation beam is tuned from 281.8 to 283 nm with a resolution of 5 pm, and each data point represents the average over 200 laser shots. The inset shows results obtained in the flame experiment used to align the LIF beam. OH is measured in the blue part of the flame at temperatures above 1' 500 K. At this temperature, the higher rotational states of OH are populated significantly up to N'' = 10, 11 and 12, and transitions $R_2(10)$, $R_1(12)$ and $R_2(11)$ appear from the flame. They are absent in the lower curve which was obtained from a pump and probe measurement of OH at room temperature in a controlled atmosphere in the reaction cell with a delay of 1 ms between the 2 laser pulses, and $[O_3]$ = 70 ppb. The fluorescence excitation spectrum of OH is necessary to check the optical resolution of the system, and to calibrate the wavelength scale of the dye laser controller.

Figure 4 presents a high resolution spectrum near the $Q_1(1)$ transition which is used in this study for the OH relaxation measurements. This envelope includes the $Q_{21}(1)$, and even the $R_2(3)$ band. The latter is not very significant, whereas the former generates a "shoulder" on the $Q_1(1)$

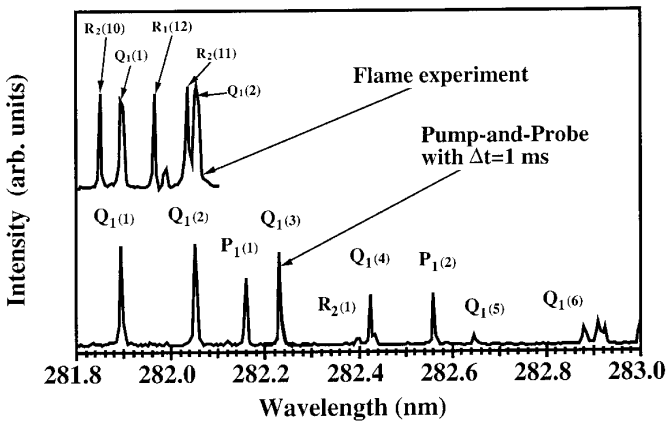

Figure 3. The OH LIF absorption spectrum measured with a delay of 1 ms between the pump and the probe beam: the ozone concentration is 70 ppb and water vapor pressure is 2%. Each data point is averaged over 200 laser shots, the probe wavelength step is 0.005 nm, and the induced fluorescence is collected at 309 nm with 4 nm bandwidth. The inset shows a similar spectrum obtained in a methane-oxygen flame where higher rotational states are measured because the temperature being above 1' 500 K.

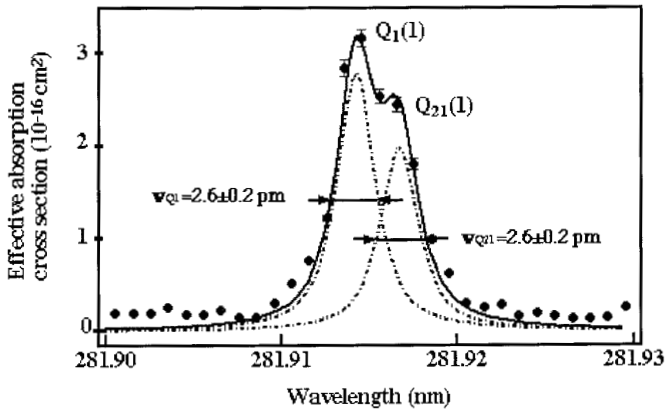

Figure 4. The effective absorption cross section obtained from high resolution absorption LIF spectrum of OH for the $Q_1(1)$ and $Q_{21}(1)$ transitions: the dotted lines show the 2 measured Voigt profiles with respectively a FWHM of the Voigt distribution w_V = (2.6 ± 0.2) pm for the $Q_1(1)$ transition and w_V = (2.6 ± 0.2) pm for the $Q_{21}(1)$ transition. The full lines represent the deconvoluted results. The data points are measured every single picometer, and the error bars are shown only for statistical errors.

transition. Two Voigt profiles have been calculated for these transitions and they are shown in figure 4. The experimental values for the FWHM of the Voigt profiles are w_V = (2.6 ± 0.2) pm for both $Q_1(1)$ and $Q_{21}(1)$ transitions. In the calculation of the effective OH cross section, we have considered a value of 3.07 pm yielding σ_{eff} (theoretical) = 2.8 × 10^{-16} cm^2. With this experimental value of (2.6 ± 0.2) pm for $Q_1(1)$, we estimate σ_{eff} (experimental) = (3.1 ± 0.4) 10^{-16} cm^2. The estimate of the OH concentration therefore changes from [OH] = (7.6 ± 2.3) × 10^{10} molecules cm^{-3} to $[OH]_{exp}$=(7.3±2.2)x10^{10} molecules cm^{-3}, which is in good agreement with the theoretical value $[OH]_{theoretical}$ = (7.2 ± 1.5) × 10^{10} molecules cm^{-3}. Because of the very narrow transition bands for OH, its measurement after the O_3 flash photolysis can be envisaged using a DIfferential Absorption LIDAR (DIAL) technique for which the [OH] will be probed with 2 laser pulses, one tuned on the maximum of the $Q_1(1)$ absorption band or the so called *on* resonance wavelength and the second tuned on the *off* resonance wavelength, but only shifted by less than 10 pm from the *on* wavelength. In a DIAL analysis, the *on* and *off* Lidar signals are used to obtain the range resolved [OH] profile [17]. Due to the very small difference between the *on* and *off* wavelengths, the OH concentration can be obtained without taking into account the wavelength dependence of the backscatter. Furthermore essentially no interference from other trace gases such as SO_2 or residual O_3 is expected. As the effective OH absorption cross section for the $Q_1(1)$ transition reaches a value of more than two orders of magnitude higher than the ozone cross section at the same wavelength, and the [OH] just after the laser flash photolysis is 6% of the initial O_3 concentration, this OH absorption in the DIAL experiment will be feasible.

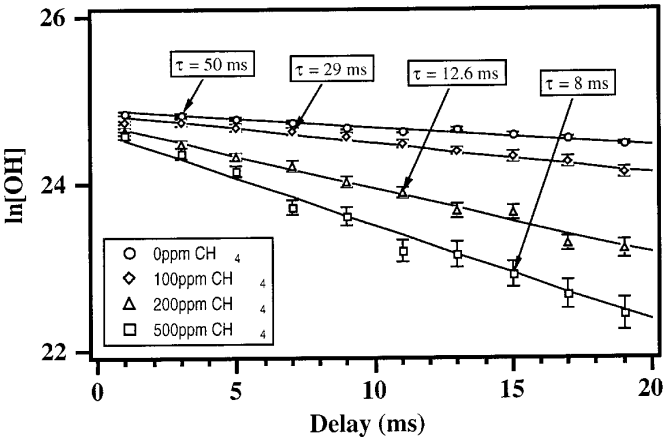

Figure 5. Natural logarithm of the OH concentration as a function of time measured in the pump and probe experiment for "clean air" conditions and for three concentrations of added methane. Each data point is an average of 500 laser shots, measured on the $Q_1(1)$ line at 281.914 nm.

So far we have shown that the pump and probe experiment appears to give a reasonable answer in the determination of the absolute [OH], as similar values are obtained in both the experimental and the simulated determinations.

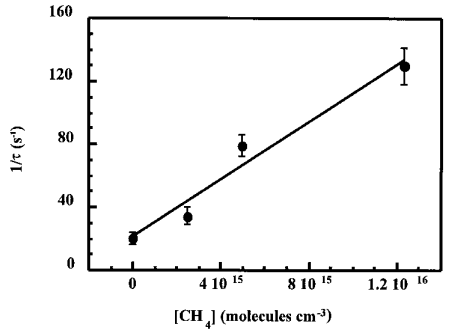

Figure 6. The inverse of the OH life-time versus the methane concentration. The slope of the fitted points gives the reaction rate constant for the reaction between CH_4 and OH at the experimental conditions.

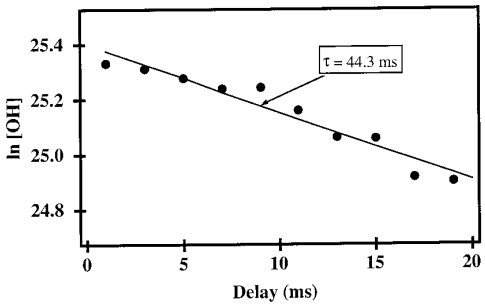

Figure 7. The natural logarithm of the OH concentration as a function of time under conditions which are essentially those of the PBL.

A second important step in the calibration of the method is the validation of the experiment in terms of chemical kinetics. Hence we selected a known chemical reaction, namely the reaction between methane and the hydroxyl radical as a test case. In figure 5, four different [OH] relaxation curves are shown in clean synthetic air flow containing no methane and respectively 100, 200 and 500 ppm CH_4 at atmospheric pressure and room temperature. Each OH data point is averaged over 500 shots, and the [OH] relaxation curve is obtained by repeating the experiment with different time delays between the pump and the probe laser. The mean OH life time $\tau(OH)_{exp}$ is obtained for each of these four curves by fitting a linear function to the slope of the natural logarithm of the signal versus time between 1 and 20 ms. For longer delays, the assumptions of a first order exponential decay of the OH signal starts to lose its validity due to the secondary formation of OH induced by the probe beam itself, and the poor S/N ratio of these preliminary experiments. With an uncertainty on each [OH] value of around 30%, the uncertainty in the OH life time $\tau(OH)_{exp}$ for the different CH_4 concentrations is increasing for the longest life time, and varies from typically 8.8% for the curve with 500 ppm CH_4 up to 17.6% for the base case without methane.

In figure 6, the inverses of the measured life times $\tau^{-1}(OH)_{exp}$ are plotted versus $[CH_4]$. For a first order reaction at $T_{reactor}$ = 296 K, the slope of the linear fit through these four points gives an upper limit to the rate constant $k_{(CH4+OH)exp} = (9.2 \pm 1.3) \times 10^{-15}$ cm^3 molecule^{-1} s^{-1}. As there may have been some slight impurities in the methane, this is not in too bad agreement with the most recent literature values of $k_{(CH4+OH)lit} = (6.3 \pm 0.6) \times 10^{-15}$ cm^3 molecule^{-1} s^{-1} [18]. One possible source of error is the relatively small dynamic range of our actual experimental set-up. Future developments to increase the sensitivity of this experiment will be twofold. First, the 8 bit AD oscilloscope acquisition unit will be replaced by a 12 bit 20 MHz AD converter, with both analog and photon counting in order to improve the signal dynamics. Second, the time scale is limited in this study to delays below 20 ms, mainly because of the secondary OH formation due to the probe beam at 282 nm. Using a new laser source probing at 308 nm for which the OH cross section is significantly higher, and the secondary formation of OH is significantly lower, this problem can be decreased. Even though our present experimental value of $k(OH+CH_4)$ is nearly 50% higher than the latest literature value, this discrepancy is nevertheless thought to be acceptable when one considers the much bigger variations in OH life time due to different types of (natural) air conditions in the PBL, as will be demonstrated below.

As the present paper only presents preliminary data and should be regarded as a proof of principle that pump and probe data can be extracted from the atmosphere, we conclude that the calibrations of the OH concentrations and the OH life times yield reasonable numbers for both the absolute OH concentrations and the reaction rate constant for a known reaction. These two procedures were carried out in a closed reaction vessel at atmospheric pressure, at room temperature, and with a flow of synthetic air containing ozone and water vapor at concentrations similar to those often encountered in the PBL. To demonstrate that such measurements can also be performed in the real PBL, we repeated the measurement of the [OH] decay, this time without the reactor vessel and directly in the air of the laboratory next to an open window. The results are presented in figure 7. These data represent our first measurement of the OH lifetime in the PBL. The ozone concentration was 66 ppb. These data show that the pump and probe OH experiment is not just another laboratory technique, but a real *in situ* method that can in principle be used in the real atmosphere. The OH life time obtained in this experiment is not interpreted here because at this point of the study, no control on the OH reactants such as NO_x or VOCs was performed. Nevertheless the OH life time obtained is of a reasonable order of magnitude.

In the following section, using a model simulation we will show what type of information might be extracted from the pump and probe technique.

Modeling the pump and probe experiment

The [OH] time dependence, from its formation by the photolysis of an ozone-water mixture to its disappearance due to atmospheric chemical reactions, is simulated with a model including the chemical and the physical properties of the atmosphere [19]. It is based on the mass conservation equation:

$$\frac{\partial C_k}{\partial t} + \vec{\nabla}\vec{U}C_k = \vec{\nabla}\left[\left(\kappa_t + \kappa\right)\vec{\nabla}C_k\right] + \dot{\omega}_k \qquad (6)$$

A B C D

where

C_k is the concentration of the k^{th} species,

$\vec{U}$ is the wind speed,

κ is the molecular diffusion,

κ_t is the turbulent diffusion,

$\dot{\omega}_k$ is the net chemical reaction rate for the k^{th} species.

Chemistry: For the chemical part of equation (6) (terms A and D), a chemical model of the troposphere including 53 chemical species and 73 reactions is applied using the CHEMKIN II package [20]. This program incorporates the temperature and pressure dependence of all important uni-, bi-, and termolecular reactions, and also explicitly takes into account the reverse of every elementary reaction. The kinetic parameters are taken from kinetic data evaluations for atmospheric chemistry or are estimated. This is a simulation of the pump and probe experiment for the OH decay curves in different air mixtures. It must be underlined that this simple model is only applied to the present experimental conditions and it is not pretended to be a complete box model for optimally simulate the real PBL. In figure 8, [OH] is given as a function of time, with a time resolution of 1 ms, the first time step treating the OH formation, i.e. the reaction of O^1D with water. The [OH] decay is treated for two types of air conditions, a "remote continental" and "moderately polluted" case. These two cases simulate air parcels that have been measured in field campaigns, for fairly clean case in Brazil and for moderately polluted case near the city of Atlanta [16,21–25]. A large difference in the observed life-time is obtained depending on both the amount of nitrogen oxides (NO_x) and volatile organic compounds (VOC) in the air: for the fairly clean case, the simulation gives an OH life time of 85.5 ms, while this value drops to 11.7 ms in the moderately polluted case where there is both high [NO_x] and high [VOC]. This result shows a rather large range for the OH time dependence for two different air pollution conditions. The results of this simulation underline the interest of the pump and probe method, and the sensitivity of the fast kinetics to the atmospheric conditions. It should be noted that this range is much larger than the uncertainty affecting our calibration test on the experimental value of the rate constant obtained for OH with methane.

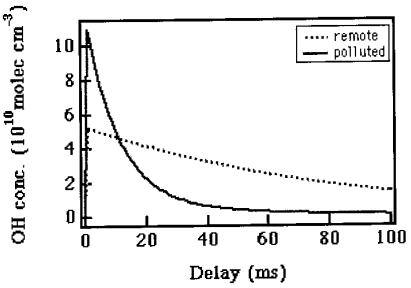

Figure 8. Simulated OH concentration *vs.* time for "moderately polluted" and "fairly clean" atmosphere (chemistry only case). See table II for the different initial concentrations used in these two cases.

Due to the very short time scale this study is addressing, a large fraction of the reactions in the model are shown to play a negligible role, in particular all the photochemical reactions. In table II are listed only the species which play a significant role in this fast OH kinetics experiment, together with their initial concentrations for the "moderately polluted" and the "fairly clean remote" cases. The initial OH concentration for the polluted case is much larger than for the clean, which is related to the initial ozone concentrations in table II, respectively 80 and 35 ppb.

For the clean case one should note that a significant residue of OH is present after 100 ms. This corresponds to the time of the next pump laser pulse under our

Table II. The list of the major species influencing the OH decay time in a time scale smaller than 20 ms, used as initial conditions for the simulated results presented in figure 8.

Species	*Remote atmosphere [ppb]*	*Polluted atmosphere [ppb]*
NO	0.1[a]	120[a]
NO_2	1[a]	100[a]
O_3	35[a]	80[a]
CO	207[b]	1000[a]
methane	1657[b]	1657[b]
formaldehyde	0.5[a]	15[d]
ethylene	0.97[b]	1.5[e]
n-butane	0.09[b]	4.2[e]
isoprene	2.65[b]	0.92[e]
myrcene	0.19[c]	0.68[f]
propylene	0.31[b]	0.5[e]

[a] Finlayson-Pitts et al., 1986, and references therein; [b] Zimmerman et al., 1988; [c] Greenberg et al., 1984; [d] Jacobson et al., 1996; [e] Chameides et al., 1992; [f] Shaw et al., 1983.

experimental conditions, and this would result in a build up of a new steady state OH concentration. Thus experimentally in such a clean atmosphere, one must reduce the repetition rate of the two lasers down to the experimental conditions at which no memory effect remains. Furthermore, these very long life times would be difficult to analyze because, as will be shown later, this chemistry could be strongly biased by the wind diffusion and turbulence effects. The relative geometry of the two beams will also be modified in order to diminish these transport effects.

A sensitivity analysis of the model calculations confirmed that a large fraction of the reactions play a negligible role in these fast kinetics. Therefore we can simplify the model resulting in a code with only those species listed in tab. II. When we compare the OH life times obtained with the "complete" set of reactions to the results with the strongly simplified model, the OH life time is equivalent within ± 5%. This holds for time scales shorter than 20 ms and for initial OH concentration lower than 10^{11} mol/cc.

Note that in the "complete" model, HO_2 formation is also included. This species could in principle interfere with the OH kinetics even on quite short time scale. This effect of HO_2 is shown to be negligible. The simpler code which does not contain HO_2 reproduces the results obtained with the more complex model quite well. For initial OH concentrations much higher than our actual values, this effect does become significant. Using the simplified chemical approach, the inverse of the predicted OH life time for a time delay shorter than 20 ms can be described as:

$$1/\tau_{OH} = k_{CO}[CO]_0 + k_{O3}[O_3]_0 + \Sigma k_{VOC}\,[VOC]_0 + \Sigma k_{NOx}\,[NO_x]_0 + 2k_{OH}[OH]_0 \qquad (7)$$

where the OH life-time τ_{OH} and its initial concentration $[OH]_0$ are obtained by the pump and probe experiment, and the only unknown is $\Sigma k_{VOC}[VOC]_{0'}$ as the measurement of the initial concentrations of $[CO]_0$, $[O_3]_0$ and $[NO_x]_0$ are obtained with standard trace gas detectors. Equation (7) is valid only for high initial [OH] and short time scales. $\Sigma k_{VOC}[VOC]_0$ is defined as the reactivity-weighted sum of all the different volatile organic compounds, a value that is otherwise not easy to obtain. We are currently investigating the possibility of using this quantity to determine if ozone production at the reaction site is NO_x limited or VOC limited.

Transport effect: To this "chemistry only" simulation, the influence of transport processes on the pump and probe experiment should be added (terms B and C in Eq. (6)). This is important in defining the conditions under which the pump and probe is feasible in real PBL conditions. Wind diffusion and turbulences influence the measured OH life time in the investigated volume and following this argument it is also important to optimize the relative geometry of the two laser beams in order to decrease the influence of the transport. The mean transport velocity moves OH out of the probed zone, and to reduce this effect, the diameter for the pump and the probe beams must be adapted depending on the scale of the transport phenomenon and the time of the measurement. In the case of the turbulent diffusion, including both the dynamic turbulence caused by the wind and the thermal turbulence caused by the differential heating of the earth's surface, the τ_{OH} measured tends to be reduced faster than with the chemical reactions alone. Under moderate atmospheric conditions, our calculation shows that OH measurements over tens of ms are possible with no influence from the wind. Indeed the influence of the wind on the measurement of residual OH mainly depends on the configuration of the laser beams. For example, in the result presented in figure 7 for the open air conditions with pump and probe beam diameter of respectively 10 and 4 mm, it is sufficient to have an averaged wind speed of 0.1 m/s to somewhat perturb the OH decay curve at delays longer than 20 ms.

Finally it should be mentioned that we are in the process of publishing the first atmospheric DIAL measurements which demonstrate the feasibility of range resolved pump and probe OH observations in the PBL [26].

Conclusions

Preliminary measurements of the reaction rate of OH radicals are presented in both a flow reactor and the real atmosphere, after the OH concentration has been raised by background ozone flash photolysis at 266 nm and reaction of the $O(^1D)$ atoms with water vapor. Detection of OH was performed by laser induced (282 nm) fluorescence (309 nm) at various time delays after the photolysis pulse. These experiments were designed to demonstrate in part the feasibility of extending such a pump and probe experiment to a range resolved atmospheric differential absorption measurement.

Kinetics measurements in the flow reactor in the presence of large amounts of methane, and a mathematical simulation of the experiment, gave values for the absolute OH concentration measured and its decay rate reasonably close to the expected values.

Experimental simulation of the fast OH decay measured in the flow system with more or less polluted artificial air mixtures, showed the sensitivity of the pump and probe measurement to air pollution changes. It is also shown that under the experimental conditions used we can measure $\Sigma k_i[OH]\,[VOC_i]$ if complementary measurements are made on CO, O_3 and NO_x. The measurements reported in this paper indicate that the range resolved pump and probe measurement is feasible. Further investigation will show if this quantity will be of interest in optimizing ozone reduction strategies [27,28].

Acknowledgements

The authors would like to thank Dr. M.J. Rossi for his contribution to the initial Chemkin calculations of this work, as well as Dr. T. Russell, Dr. S. Sillman, and Dr. A.

Hofzumahaus for valuable discussions. This work is supported by the Swiss National Science Foundation.

References

1. O'Brien, R. J.; Hard, T. M. Tropospheric hydroxyl radical, Measurement challenges in atmospheric Chemistry, Advances in Chemistry, Series 232, L. Newman, 1993; pp 323-371.
2. TOHPE, *J. Geophys. Res.* **1997**, *102* (*D5)*, 6169-6510.
3. Brock, J. C.; Watson, R. T. *Chem. Phys. Lett.* **1980**, *71*, 371.
4. Molina, L. T.; Molina, M. J. *J. Geophys. Res.* **1986**, *91* (D13), 14, 501-14, 508.
5. Atkinson, A.; Baulch, D. L.; Cox, R.A.; Hampson Jr., R.F.; Kerr, J.A.; Rossi, M.J.; Troe, J. *J. Phys. Chem. Ref. Data* **1997a**, *26*(2).
6. Wine, P. H.; Ravishankara, A. R. *Chem. Phys. Lett.* **1981**, *77(1),* 103-109.
7. Brune, W. H.; Stevens, P. S.; Mather, J. H. *J. Atmos. Sci.* **1995**, *52,* 3328-3336.
8. Crosley, D. R. *J. Atmos Sci.* **1995**, *52*, 3299-3314.
9. Dorn, H. P.; Brandenburger, U.; Brauers, T.; Hausmann, M. *J. Atmos. Sci.* **1995a**, *52*, 3373-3380.
10. Hard, T. M.; George, L. A.; O'Brien, R. J. *J. Atmos. Sci.* **1995,** *52*, 3354-3372.
11. Holland, F.; Hessling, M.; Hofzumahaus, A. *J. Atmos. Sci.* **1995**, *52*, 3393-3401.
12. Tanner, D. J.; Eisele, F. L. *J. Geophys. Res.* **1995**, *100*, 2883-2892.
13. Dorn, H. P.; Neuroth, R.; Hofzumahaus, A. *J. Geophys. Res.* **1995b**, *100*(D4), 7397-7409.
14. Whiting, E. E. *J. Quant. Spectrosc. Radia. Transfer*. **1968**, *8*, 1379-1384.
15. McGee, T. J.; McIlrath, T.J. *J. Quant. Spectrosc. Radia. Transfer* **1984**, *32*, 179-184.
16. Finlayson-Pitts, B. J.; Pitts, J. N. Atmospheric chemistry: fundamentals and experimental techniques, A Wiley-Interscience Publication, John Wiley & Sons, 1986.
17. Schoulepnikoff, L.; van den Bergh, H.; Calpini, B.; Mitev, V. Tropospheric air pollution monitoring, LIDAR; Encyclopedia of Environmental Analysis and Remediation, Meyers Editor, John Wiley & Sons, 1998.
18. Atkinson, A. *J. Phys. Chem. Ref. Data* **1997b**, *26*(2) 215-290.
19. Clappier, A.; Calpini, B.; Durieux, E.; Fiorani, L.; Jaquet, L.; van den Bergh, H. 1994, Numerical study of pump and probe LIDAR experiment for in situ tropospheric measurement of the OH radical, Proc. of 17th International Laser Radar Conference, Sendai, Japan.
20. Kee, R. J.; Rupley, F. M.; Miller, J. A. 1991, CHEMKIN-II: A fortran chemical kinetics package for the analysis of gas-phase chemical kinetics, Sandia Report, Sandia National Laboratories, USA.
21. Zimmerman, P. R.; Greenberg, J. P.; Westberg, C. E. *J. Geophys. Res.* **1988**, *93*(D2), 1407-1416.
22. Greenberg, J. P.; Zimmerman, P. R. *J. Geophys. Res.* **1984**, *89* (D3), 4767-4778.
23. Jacobson, M. Z.; Lu, R.; Turco, R. P.; Toon, O. B. *Atmos. Environ.* **1996**, *12*, 1939-1963.
24. Chameides, W. L.; Fehsenfeld, F.; Rodgers, M. O.; Cardelino, C.; Martinez, J.; Parrish, D.; Lonneman, W.; Lawson, D. R.; Rasmussen, R. A.; Zimmerman, P.; Greenberg, J.; Middleton, P.; Wang, T. *J. Geophys. Res.* **1992**, *97*(D5), 6037-6055.
25. Shaw, R. W.; Crittenden, A. L.; Stevens, R. K.; Cronn, D. R.; Titov, V. S. *Environ. Sci. Technol.* **1983**, *17,* 389-396.
26. Jeanneret et al., to be published.
27. Chameides, W. L.; Cowling, E. B. 1995, The state of the Southern Oxidants Study (SOS): Policy-relevant findings in ozone pollution research 1988-1994, Raleigh.
28. Calpini, B.; Simeonov, V.; Jeanneret, F.; Kuebler, J.; Sathya, V.; van den Bergh, H. *Chimia* **1997**, *51*, 700-704.
29. Burris, J.; Butler, J. J.; McGee, T. J.; Heaps, W. S. *Chem. Phys.* **1988**, *124*, 251-258.
30. Chan, C. Y.; O'Brien, R. J.; Hard, T. M.; Cook, T. B. *J. Phys. Chem.* **1983**, *87*, 4966-4974.
31. Dieke, G. H.; Crosswhite, H. M. *J. Quant. Spectrosc. Radia. Transfer*. **1962**, *2*, 97-199.
32. Williams, L. R.; Crosley, D. R. *J. Chem. Phys.* **1996**, *104*, 6507-6514.